Surface Science 651 (2016) 51–56

Contents lists available at ScienceDirect

Surface Science

journal homepage: www.elsevier.com/locate/susc

# Influence of surface defects on superlattice patterns in graphene on graphite

Maja Remskar *, Janez Jelenc

*Solid State Physics Department, Jozef Stefan Institute, Jamova 39, SI-1000 Ljubljana, Slovenia*

ARTICLE INFO

*Article history:*
Received 29 October 2015
Received in revised form 29 January 2016
Accepted 6 March 2016
Available online 11 March 2016

*Keywords:*
Graphene
Superstructure
Scanning tunnelling microscopy
Moiré pattern
Charge modulation

ABSTRACT

Superstructures observed by scanning tunnelling microscopy on graphite have been reported several decades ago, but the interest in these superstructures recently intensified due to their occurrence in graphene grown on different substrates. Generally accepted explanation of origin of these superstructures is an overlap of disoriented top layer of graphite and the underlying graphite single crystal, which causes moiré pattern. Here we present experimental findings that the orientation of the superstructure is influenced by surface defects and edges of graphene. Superstructures in graphene put on graphite exist even if the graphene is not supported by graphite over its entire area. The modulation of the density of states influences the strength of intra-layer carbon bonds in such a way that the graphene breaks along the superstructure minima. The tunnelling conductance of the areas with superstructures is enhanced with regard to bulk graphite.



## 1. Introduction

The superstructures observed by scanning tunnelling microscopy (STM) on graphite have been reported already several decades ago [1]. The explanation of the origin of the superstructures has been proposed as the overlap between a disoriented top layer of graphite and the underlying graphite single crystal, which causes a moiré pattern. This model is based on three-dimensional tunnelling of electrons with Fermi energy of the same order as the work function of a typical layered material with weak interlayer interaction [2]. Strong corrugation amplitude of the tunnelling current from the superstructure in comparison with atomic corrugation was explained by zero decay of the nanoscale waves produced by scattering at the interface in the lattice-mismatched systems. Due to a low attenuation of the nanoscale waves, the superstructure in STM can be visible at heights around one monolayer above the top surface. Several other explanations of the superstructures were proposed by different authors and reviewed [3], such as network of dislocations, physical surface deformation, a multiple tip effect, adsorption of impurities, bond shortening, and nanoscale defects buried a few layers below the surface.

Intensified interest in the scientific community for these superstructures stems from their occurrence in graphene grown on different substrates, such as silicon carbide [4,5], rubidium [6], nickel [7], iridium [8], copper [9], and hexagonal boron nitride as an isostructural crystal to graphene. These Van der Waals heterostructures allow for the tuning of the electronic properties of two-dimensional atomic crystals, particularly of graphene, creation of unique systems for adsorption of clusters [10] as quantum dots arrays [11], and they represent a way of studying the fractal quantum Hall effect [12–14]. The brightest spots of the superstructure in the STM image with the maximum density of states can also represent adsorption sites for cationic atoms or molecules [10]. Moiré patterns of graphene on hexagonally packed surfaces were also studied theoretically [15]. Besides forming moiré superstructures, orientation mismatch of graphene flakes on graphite strongly reduces friction on atomic scale. Extremely low friction was observed for incommensurate relationship of two graphite layers [16]. Transition back to commensurate ground state is triggered by thermal fluctuations and performed with superlubric gliding or rotation [17]. Understanding of interaction between graphene flakes and substrate is of a great importance for their applications in nanomechanical systems.

Here we present experimental data obtained by STM studies of graphene flakes partially peeled off bulk graphite. We show that the superstructure lattice is influenced by surface and edge defects of graphene and vice versa, that the superstructure influences how graphene breaks. These findings represent a new insight into this old phenomenon with novel implications for graphene-based technology.

## 2. Methods

The STM studies have been performed at room temperature in ultra high vacuum (base pressure in the range of $10^{-10}$ mbar) using the AFM/STM microscope (VT-AFM, Omicron). Mechanically cut Pt/Ir tips have been used. The STM tip was biased, while the sample was grounded. The superstructures have appeared occasionally during use of graphite

* Corresponding author.
*E-mail address:* maja.remskar@ijs.si (M. Remskar).

http://dx.doi.org/10.1016/j.susc.2016.03.008
0039-6028/

as a substrate for studies of different nanomaterials, such as $MoS_2$ based nanoflakes and nanotubes, $WO_x$ nanowires and $Mo_6S_6I_2$ nanocrystals. The graphite single crystals were always freshly air cleaved using adhesive tape before ethanol suspension of the nanomaterials was drop casted. Then the samples were dried at 60 °C in air and inserted into the UHV chamber in standard way. The graphite single crystals HOPG SPI-1 Grade, 10 × 10 × 1 mm, Mosaic spread angle: 0.4° ± 0.1°, purity = 99.99, dimension: 10 mm × 10 mm × 1 mm, and the absolute ethanol, purity = 99.9, M = 46.07 g/mol, used in sample preparation were purchased at SPI supplies, West Chester, USA, and MERCK, respectively. All STM images taken in constant current mode are shown after applying line-by-line and planar background subtraction. No other image filtration or rotation was used. Scan direction corresponded to x-axis of an image.

## 3. Results and discussion

### 3.1. Graphene lying over surface imperfections

Fig. 1 shows a graphene flake lying over several surface ripples and a hole. The surface above the diagonal dotted line in the Fig. 1a reveals a trigonal superstructure with a period of 3.6 ± 0.2 nm (Fig. 1b). The deepness of the hole estimated from the line profile along the ripple is 0.4 ± 0.1 nm (Fig. 1c). This value approximately corresponds to the monolayer thickness of graphite (0.3354 nm). Line profile along the superstructure lattice (Fig. 1d) reveals a depletion of 0.35 to 0.4 nm at the valley of the ripple. The shape of the superstructure maxima is sinusoidal, while the minima are tip shaped. The corrugation was 500 pm ± 100 pm over the hole, 250 pm ± 50 pm over the valleys of the ripples, and 230 pm ± 50 pm over the convex areas of the ripples. At the left side of the image (Fig. 1a) the dotted boundary is attached to a corner (A) where two monolayers have been removed during cleavage of the graphite. The dotted line is boundary of the modulation. Corrugation of the dots is 1 nm ± 0.1 nm.

Shape of the hole's edge is blurred by a strong contribution from the density of states from the superstructure. Right edge of the hole (marked with B) is in line with serial features forming a 3 × 1 (or 6 × 1) giant superstructure (C) shown in the Fig. 1a. Origin of this giant superstructure is not known. Based on geometry, one can speculate that edge states of the hole interact with tunnelling current from moiré interface and trigger its periodic modulation. It is not clear where the hole is situated, but it is either in the second layer below the surface (I to III) or in the top layer (IV), schematically presented in the Fig. 2. The first three variants are more likely and II and III are of equal possibility due to blurred edges of the hole. The fact that the edges of the hole are parallel to the moiré superstructure, suggests that the layer with the hole is one of the layers of the interface creating the moiré superstructure and the model IV is less likely.

If the image is explained by the standard moiré model, which is based on mismatch and/or rotational disorder interface (moiré interface), then the interface would be buried three (I), two (II) or one (III) layers below the top surface. The defects in the topmost layer obviously affect the density of states at the moiré interface situated several monolayers below the surface. The corner (A) has an effect on the interface below the surface, and the edge of the hole (B) influences the orientation of the super structure lattice. The influence of surface

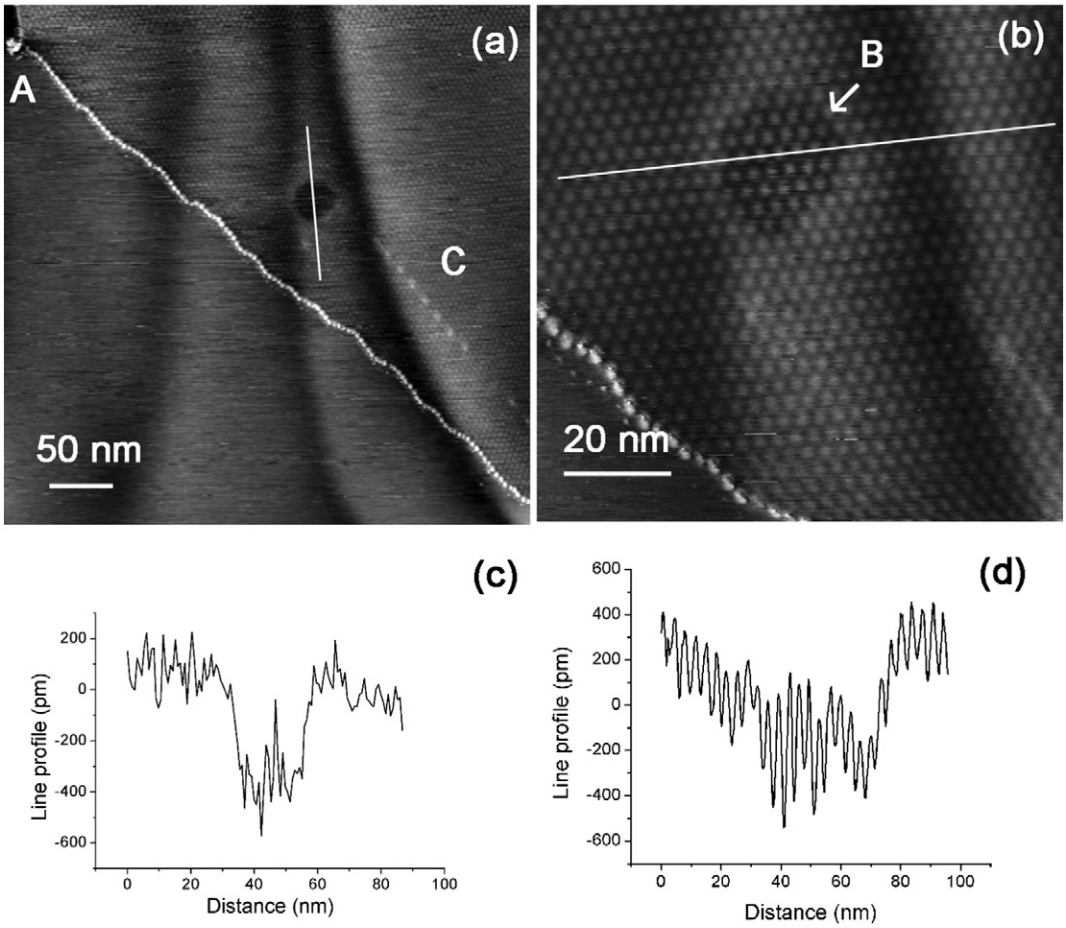


**Fig. 1.** a) Graphene flake lying over several surface ripples and over a hole ($U_T = 0.5$ V, $I_T = 0.5$ nA, Z-Range: 3.28 nm; speed: 300 nm/s); b) Trigonal distribution of superstructure maxima, 3.6 nm in period ($U_T = 0.5$ V, $I_T = 0.5$ nA; Z-Range: 2.27 nm; speed: 100 nm/s); c) Line profile along the ripples crossing the hole in direction along the ripples (shown in (a)); d) Line profile along the superstructure maxima (shown in (b)).

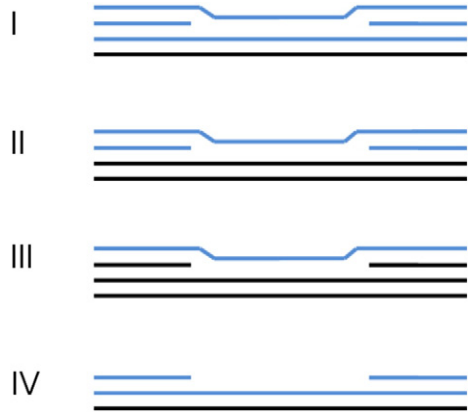


**Fig. 2.** Schematically presented stacking of graphene layers with moiré interface between blue and black lines.

defects on deeply buried moiré interface has not yet been reported yet and it is not considered in the standard moiré model [15].

The Fig. 3 shows a triple-junction (J) of the dotted lines (I, II, III) attributed to grain boundaries of graphene flakes, which are not necessary mutually rotated [18]. The boundary lines connect at angles 90°, 120°, and 150° on a surface with many cleavage steps. The boundary line I crosses two monolayers (i, ii); the first one exactly in the corner (Fig. 3a). The boundary line (II) is visible also at the area, where a part of double-layer was removed (arrow) and through the folded flake (F) shown in the Fig. 3b. Period of the dots is 2.7 ± 0.1 nm and height of 0.4 ± 0.01 nm. One should note that the boundary line II crosses the fold exactly at its edge. Next to the boundary line, the superstructure was not visible under the operating conditions (0.5 V, 0.5 nA). Line profiles perpendicularly to the dotted line (Fig. 3b-inset) show that the dotted line cannot be explained as an edge of surface flake, but it originates from the crystal inside and could be a boundary line of hidden superstructure. Fig. 3 demonstrates that the position of the boundary lines depends on the defects in the top layer.

### 3.2. Damaged top layer

The influence of surface defects to development of the superstructure is also presented in the Fig. 4a, which shows two large areas of superstructure with the period of 10.5 nm ± 0.4 nm. The image can be explained by moiré interface situated only a monolayer below the top surface and not deeply inside the substrate as in the previous examples. A part of the top layer, which has been peeled off does not show any superstructure (Fig. 4b), while the part lying over the other flake shows a strongly attenuated superstructure (* in the Fig. 4a). The edges of the peel off are parallel with the superstructure lattice. This indicates that the superstructure influences the mechanical stability of graphene. Breaking of the top layer along the superstructure reveals that the charge modulation affects the strength of intra-layer carbon bonds, which has not been evidenced before.

### 3.3. Confined superstructure

Fig. 5a shows a nanoribbon, 72 nm wide and 0.70 nm ± 0.05 nm in thickness, which can be explained as overlapped graphene bilayer. A strong enhancement of the density of states at the ribbon edges reveals as 1.8 ± 0.1 nm high peak in the line profile (Fig. 5b-inset). Surrounded by both longitudinal edges, modulation of the density of states is visible, forming a distorted trigonal superstructure with the period of 14.3 ± 0.5 nm measured along the direction of the scanning. The ribbon edge was rotated 52° with respect to the direction of the scanning. One line of the superstructure maxima is oriented in parallel with the ribbon edge, another in parallel with the scan direction, and the third rotated for 60° with respect to the ribbon edge. In contrast with nearly ideal hexagonal lattice described in Figs. 1 and 3, the superstructure lattice on the surface of the ribbon is slightly distorted from trigonal symmetry. The distortion is not caused by scan drift, because different scan speeds or direction of scanning (forward, backward) did not change it. If this superstructure is explained as a rotational moiré forming at the interface between both walls of the ribbon, the ribbon should be rotated with respect to the underlying layers by 0.99° according to the moiré equation valid for a rotational disorder of two identical crystals: $D = p/2/[\sin(\alpha/2)]$, where D is period of the moiré superlattice, p is the lattice parameter, and α is angle of rotation. This small angle prevents explicit explanation of the origin of the superstructure because the longitudinal end of the ribbon seems perfectly aligned with the underlying flake (Fig. 5a). Occurrence of the moiré superstructure as a consequence of strain induced lattice mismatch is also possible [19].

### 3.4. Scanning tunnelling spectroscopy studies

The Fig. 6 shows a current image (constant height mode) of superstructure with a period of 10.2 nm ± 0.5 nm. Thin graphene flake crosses a black line (arrow), which can be explained as 8 ± 1 nm

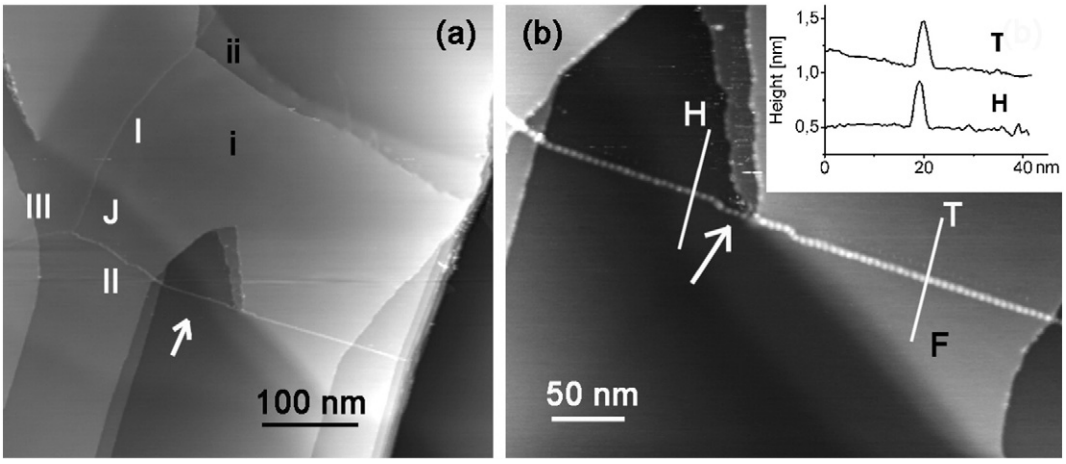


**Fig. 3.** Triple-junction J of three boundary lines (I, II, III) of unresolved superstructure: a) line I crossing two monolayers (i, ii); the first one exactly in the corner, where graphite monolayer was removed. Line II visible also at the area, where a part of double-layer was removed (arrow) ($U_T = 0.5$ V, $I_T = 0.5$ nA; Z-Range: 6.44 nm; speed: 600 nm/s); b) Modulation of the boundary line II, 2.7 ± 0.1 nm in period, which crosses the folded flake (F) exactly at its edge ($U_T = 0.5$ V, $I_T = 0.5$ nA; Z-Range: 1.96 nm; speed: 200 nm/s); inset: two line profiles at the hole (H) and terrace (T) areas.

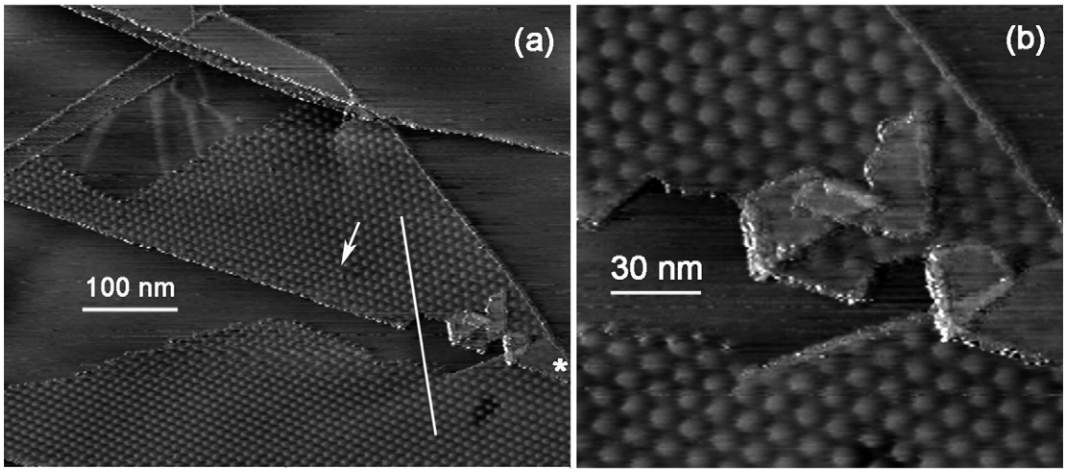


**Fig. 4.** A superstructure, 10.5 nm in period: a) Two large areas with superstructure lattices, which are out of phase in both flakes. Arrow points the end of a line dislocation in the superstructure ($U_T = 0.5$ V, $I_T = 0.3$ nA; Z-Range: 9.14 nm; speed: 600 nm/s); b) A broken graphene along the superstructure minima ($U_T = 0.5$ V, $I_T = 0.3$ nA; Z-Range: 9.17 nm; speed: 300 nm/s).

deep crack in the top layer. The modulation intensity of the current in the superstructure is enhanced near the crack and the superstructure lattice is strongly deformed (Fig. 6b). The superstructure period of 10.2 nm was measured along direction pointed by arrow in the Fig. 6b.

Scanning tunnelling spectroscopy was performed on the flake in the 3 nm-raster mode from −150 mV to 150 mV with 50 ms acquisition time. Simultaneously, the STM topography image was recorded at $U_T = 0.2$ V, and $I_T = 0.3$ nA. The trigonal symmetry in the topography image (Fig. 6c) is strongly deformed with respect to Fig. 6b because of a scan drift during the lasting spectroscopy measurement. Nevertheless, the maxima and minima of the superstructure are resolved, as well as the modulation of the density of states at the edge of the superstructure. The spectroscopy data were collected at the minima (a) and maxima (b) of the superstructure, and on graphite (c) near the superstructure. The current–voltage characteristics shown in the Fig. 6d reveal a metallic behaviour at all three locations with the highest tunnelling conductance at the maxima of the superstructure and the smallest at HOPG. Larger differences in the conductance are observed at negative tip biases (unoccupied states).

## 4. Discussion

The superstructures observed on the surface of graphite cannot be explained solely by the generally agreed moiré pattern, which considers only interface between mutually rotated top layer and the underlying substrate. The superstructure was visible in the graphite monolayer flake (graphene) lying on graphite which contained surface imperfections, and also on a graphene ribbon-like structure. The superstructure was clearly visible in areas in the Fig. 1, where graphene was lying over ripples or holes. Considering that the topmost graphene due to irregular shape of the rippled graphite layer cannot be one of the rotated planes causing the regular moiré pattern, the moiré interface should be at least three monolayers below the surface. The attenuation factor (AF) is defined as the ratio between the corrugation of a moiré pattern at its origin and a moiré pattern covered by $n$ over layers according to the equations: $AF_n = e^{0.81n}$ [20] or $AF_n = 2^n$ [21]. Using these equations the corrugation amplitudes of the superstructure inside the hole and in area surrounding the hole were compared. The AF at the convex areas around the hole is found 2. This value corresponds to one over layer [21]. The AF factor for the concave areas is only 1.2, which corresponds

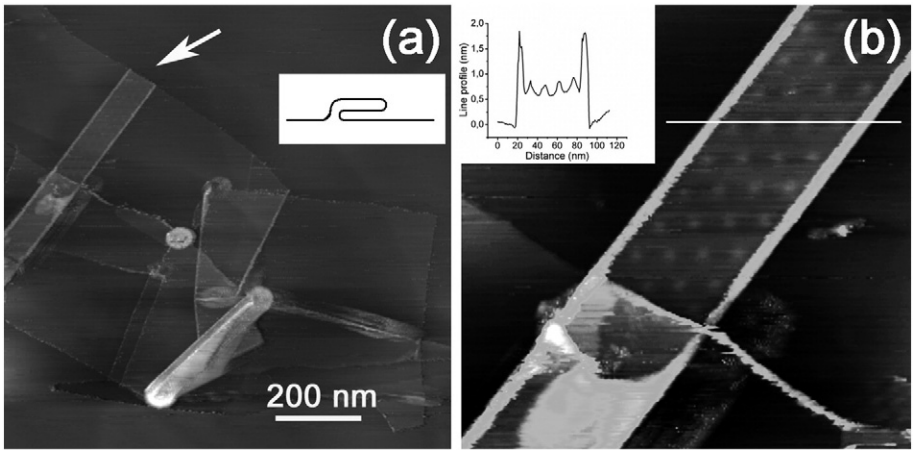


**Fig. 5.** a) The 0.7 nm thick ribbon-like fold (arrow) ($U_T = 0.5$ V, $I_T = 0.5$ nA, Z-Range: 10.35 nm; speed: 800 nm/s); b) A superstructure, 14.3 ± 0.5 nm in period, developed inside the ribbon and oriented in parallel with its longitudinal edge ($U_T = 0.5$ V, $I_T = 0.5$ nA, Z-Range: 5.73 nm; speed: 200 nm/s). Inset shows a line profile crossing the ribbon along the scan direction.

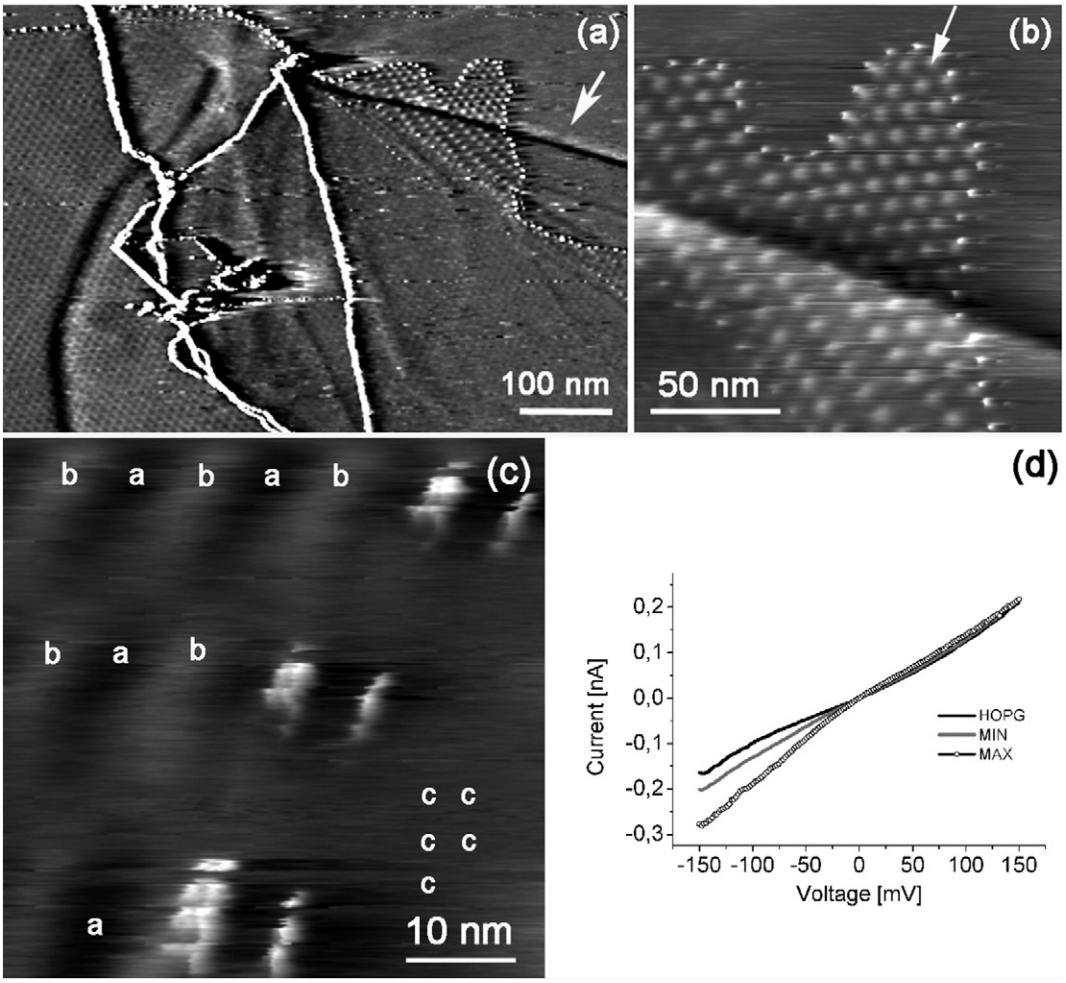


**Fig. 6.** a) A graphene flake crossing the 8 ± 1 nm deep surface crack (arrow) ($U_T = 0.2$ V, $I_T = 0.3$ nA, Z-Range: 3.33 nA; speed: 800 nm/s); b) Deformed lattice of the superstructure at the transition over the crack ($U_T = 0.2$ V, $I_T = 0.3$ nA, Z-Range: 17 nm; speed: 200 nm/s); c) Locations of the spectroscopy measurement on the part of the flake shown in the Fig. 6b: minima of the superstructure marked with (a), maxima with (b) and graphite near the superstructure with (c), ($U_T = 0.2$ V, $I_T = 0.3$ nA, Z-Range: 12.23 nm; speed: 45 nm/s); d) Current–voltage characteristics (I–V) taken at the superstructure minima (MIN), maxima (MAX) and on graphite (HOPG).

to 0.25% of the monolayer thickness, and is in agreement with explanation as ripples. The period of the modulation is not affected by the presence of a hole or ripples.

Several cases of matching positions of the superstructure lattice and surface imperfections were found, like those presented in the Figs. 1, 3 and 4. These results cannot be explained by the moiré model of three dimensional tunnelling from moiré interface inside the crystal toward the top surface, if surface states are not considered. Questions like how the defects in the topmost layer affect the density of states three layers below the surface, or why the top layer would break along minima of superstructure which originates deeply within the substrate, remain open.

The superstructure which developed in the ribbon-like flake of graphene and aligned along the longitudinal edge of the fold cannot be explained by the rotational disorder inside the ribbon (Fig. 5). The alignment of the longitudinal end of the ribbon-like flake with the edge of the supporting flake opposes such an explanation. The possibility that a kind of ribbon-like graphene flake buried inside graphite, which would originate the moiré pattern is also unlikely.

Scanning tunnelling spectroscopy (Fig. 6d) has shown that the tunnelling conductance measured at both, the maximum (MAX) and minimum (MIN) sites of the superstructures, is larger than the tunnelling conductance of HOPG at the negative tip biases, when unoccupied states are revealed. We believe that modulation of density of states at moiré interface, particularly of unoccupied states, is influenced by point or line defects on the top surface. One should note that the superstructures appeared only when a graphene flake was limited in the basal area. The superstructure is visible inside a limited range of applied voltages and only by STM. Further discussion regarding the theoretical explanation of graphitic superstructure is needed.

## 5. Conclusions

The STM studies of superstructures observed on graphene flakes which have been split from graphite, have shown that the defects in the top-surface layer affect the orientation of the superstructure. Such a strong interaction between surface imperfections, like ribbon-like flakes, holes or steps, and the so-called moiré superstructure, has not been reported yet. The scanning tunnelling spectroscopy has revealed an enhancement of the tunnelling conductance of the whole area with superstructures with regard to graphite, particularly on account of unoccupied energy states. The largest tunnelling conductivity was found in maxima of the superstructure. The modulation of the density of states caused by development of superstructure influences the strength of the intra-layer bonds of carbon atoms in a way that graphene breaks along the superstructure minima. These findings are important for construction of devices based on graphene.

## Acknowledgements

The authors acknowledge support from the Slovenian Research Agency (No. P1-0099).

## References

[1] M. Kuwabara, D.R. Clarke, D.A. Smith, Appl. Phys. Lett. 56 (1990) 2396.
[2] K. Kobayashi, Phys. Rev. B 53 (1996) 11091.
[3] W.T. Pong, C. Durkan, J. Phys. D. Appl. Phys. 38 (2005) R329.
[4] W.A. Van de Heer, C. Berger, X. Wu, M. Sprinkle, Y. Hu, M. Ruan, et al., J. Phys. D. Appl. Phys. 43 (2010) 374007.
[5] K. Yagyu, T. Tajiri, A. Kohno, K. Takahashi, H. Tochihara, H. Tomokage, et al., Appl. Phys. Lett. 104 (2014) 053115.
[6] D. Stradi, S. Barja, C. Diaz, M. Garnica, B. Borca, J.J. Hinarejos, et al., Phys. Rev. B 88 (2013) 245401.
[7] A. Dahal, M. Batzill, Nanoscale 6 (2014) 2548.
[8] S. Standop, T. Michely, C. Busse, J. Phys. Chem. C 119 (2015) 1418.
[9] P. Süle, M. Szendrő, C. Hwang, L. Tapasztó, Carbon 77 (2014) 1082.
[10] J. Xhie, K. Sattler, M. Ge, N. Venkateswaran, Phys. Rev. B 47 (1993) 15835.
[11] G. Li, L. Huang, W. Xu, Y. Que, Y. Zhang, J. Lu, et al., Constructing molecular structures on periodic superstructure of graphene/Ru(0001), Phil. Trans. R. Soc. A 372: 20130015.
[12] L.A. Ponomarenko, R.V. Gorbachev, G.L. Yu, D.C. Elias, R. Jalil, A.A. Patel, et al., Nature 497 (2013) 594.
[13] B. Hunt, J.D. Sanchez-Yamagishi, A.F. Young, M. Yankowitz, B.J. LeRoy, K. Watanabe, et al., Science 340 (2013) 1427.
[14] C.R. Dean, L. Wang, P. Maher, C. Forsythe, F. Ghahari, Y. Gao, et al., Nature 497 (2013) 598.
[15] P. Zeller, S. Günther, New J. Phys. 16 (2014) 083028.
[16] M. Dienwiebel, N. Pradeep, S.G. Verhoeven, H.W. Zandbergen, J.W.M. Frenken, Surf. Sci. 576 (2005) 197.
[17] X. Feng, S. Kwon, J.Y. Park, M. Salmeron, ACS Nano 7 (2013) 1718.
[18] Y. Wang, Y. Ye, K. Wu, Surf. Sci. 600 (2006) 729.
[19] C.R. Woods, L. Britnell, A. Eckmann, R.S. Ma, J.C. Lu, H.M. Guo, et al., Nat. Phys. 10 (2014) 451.
[20] W.T. Pong, C. Durkan, Jpn. J. Appl. Phys. 44 (2005) 5443.
[21] F.I. Dalidchik, M.V. Grishin, S.A. Kovalevskii, Phys. Low-Dimens. Struct. 3 (4) (2003) 45.